







Utilizing the Neglected Back Lobe for Directional Charging Scheduling

Tang Liu , *Member, IEEE*, Meixuan Ren , *Student Member, IEEE*, Dié Wu , Jing Xue , Jingwen Li , Sun Mao , and Wenzheng Xu , *Member, IEEE*

Abstract—Benefitting from the breakthrough of wireless power transfer technology, the lifetime of Wireless Sensor Networks (WSNs) can be significantly prolonged by scheduling a mobile charger (MC) to charge sensors. Compared with omnidirectional charging, the MC equipped with directional antenna can concentrate energy in the intended direction, making charging more efficient. However, all prior arts ignore the considerable energy leakage behind the directional antenna (i.e., back lobe), resulting in energy wasted in vain. To address this issue, we study a fundamental problem of how to utilize the neglected back lobe and schedule the directional MC efficiently. Towards this end, we first build and verify a directional charging model considering both main and back lobes. Then, we focus on jointly optimizing the number of dead sensors and energy usage effectiveness. We achieve these by introducing a scheduling scheme that utilizes both main and back lobes to charge multiple sensors simultaneously. Finally, extensive simulations and field experiments demonstrate that our scheme reduces the number of dead sensors by 49.5% and increases the energy usage effectiveness by 10.2% on average as compared with existing algorithms.

Index Terms—Back lobe, directional charging scheduling, wireless power transfer, wireless rechargeable sensor networks.

I. INTRODUCTION

ENERGY limitation is widely recognized as a key hurdle that stunts the adoption of Wireless Sensor Networks (WSNs) [1], [2]. Recently, the breakthrough of wireless power transfer [3] technology gave birth to the concept of Wireless Rechargeable Sensor Networks (WRSNs) [4], [5], [6], [7], [8] and made it received widespread attention. In WRSNs, a mobile charger (MC) is usually employed to visit and recharge

Manuscript received 26 May 2023; revised 4 September 2023; accepted 15 November 2023. Date of publication 28 November 2023; date of current version 7 May 2024. This work was supported in part by the National Natural Science Foundation of China under Grants 62072320, 62002250, 62272328, 62241108, and 62306201, in part by the Natural Science Foundation of Sichuan Province under Grants 2022NSFSC0569 and 2022NSFSC0479, and in part by the Key R&D Program of Sichuan Province under Grant 22ZDZX0021. Recommended for acceptance by K. R. Chowdhury. (*Corresponding author: Wenzheng Xu.*)

Tang Liu, Dié Wu, Jing Xue, Jingwen Li, and Sun Mao are with the College of Computer Science, Sichuan Normal University, Chengdu, Sichuan 610101, China, and also with the Visual Computing and Virtual Reality Key Laboratory of Sichuan Province, Sichuan Normal University, Chengdu, Sichuan 610068, China (e-mail: liutang@sicnu.edu.cn; wd@sicnu.edu.cn; xuejing@stu.sicnu.edu.cn; lijingwen@sicnu.edu.cn; sunmao@sicnu.edu.cn).

Meixuan Ren is with the State Key Laboratory for Novel Software Technology, Nanjing University, Nanjing 210023, China (e-mail: meixuanren@smail.nju.edu.cn).

Wenzheng Xu is with the College of Computer Science, Sichuan University, Chengdu, Sichuan 610065, China (e-mail: wenzheng.xu@scu.edu.cn).

Digital Object Identifier 10.1109/TMC.2023.3334518

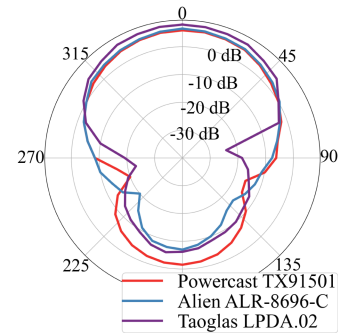


Fig. 1. Radiation patterns of three typical directional antennas produced by Powercast, Alien, and Taoglas.

energy-critical sensors, such that the operational lifetimes of sensors can be significantly prolonged. Although WRSNs have many potentials in various application scenarios (e.g., environmental monitoring [9], healthcare [10], and transportation [11]), there still exists a gap between energy supply and practical demand.

A key reason for this gap is that the energy radiated by MC is not fully utilized. Traditional wireless charging arts [12], [13], [14], [15], [16], [17], [18], [19], [20], [21], [22], [23], [24] usually employ omnidirectional antennas, which broadcast electromagnetic waves equally in all directions regardless of the location of the sensors, in this case, merely a small part of the energy could be transferred to the sensors. Instead, directional antennas concentrate the energy in the intended narrow direction via energy beamforming [25], [26], [27], [28], [29], [30], [31], [32], [33], [34], and thus enhance the energy transferred to the sensors. Nevertheless, the energy radiated by MC is still underutilized, as an unignorable part of the energy is “leaking” in unintended directions for almost all directional antennas [35].

Fig. 1 depicts the radiation patterns of three typical commercial off-the-shelf directional antennas [36], [37], [38]. It shows that in front of each directional antenna, there is an energy beam with maximum energy intensity, *aka* the *main lobe* [35]. Besides, in other directions of each antenna, there are some smaller energy beams, also called the *side lobes*, among which the extremely important one directly behind the main lobe is the *back lobe* [35]. To further demonstrate the energy radiation pattern of directional antenna in different directions, we take Powercast TX91501 [36] as an example and plot its energy distribution in Fig. 2. It can be observed that the farthest charging distance of the back lobe

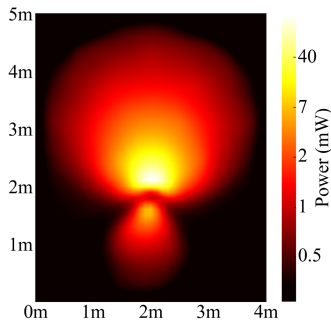


Fig. 2. Charging energy heatmap of TX91501 wireless charger produced by Powercast.

is up to 50% of that of the main lobe. Moreover, the energy intensity of the back lobe is about 20% of that of the main lobe at the same transmission distance. Even though much effort has been devoted to concentrate all the radiated energy on the main lobe [39], [40], [41], energy leakage is inevitable. As a result, a considerable amount of energy leaking behind the directional antenna is wasted in vain.

Although there are some arts focusing on the directional charging scheduling [29], [30], [31], none of them pay attention to the back lobe. All these studies design charging scheduling schemes according to the charging range and energy intensity of the main lobe. Therefore, these schemes do not effectively utilize the leaked energy behind the MC. Assuming that both the main and back lobes are utilized, in this case, a larger charging range of the MC means that more sensors have a greater chance to be charged simultaneously, thereby reducing the number of dead sensors. Meanwhile, more radiated energy from the MC can be received by sensors, thus improving the energy usage effectiveness (*EUE*). In summary, it is necessary to model the charging range and energy intensity of both the main and back lobes, and accordingly design a charging scheduling algorithm.

In this paper, we focus on making full use of the energy of the main and back lobes to improve charging performance. In particular, we study the problem of directional charging scheduling with main and BACK lobes (BACK), i.e., how to use a directional MC to travel and stop at several candidate locations with proper orientations to charge sensors so that the number of dead sensors is minimized and *EUE* is maximized. Generally, we are faced with two major challenges.

The first challenge is how to build a charging model with both main and back lobes that accurately describes the characteristics of the directional MCs. Unlike the main lobe, the manufacturers do not provide the parameters of the back lobe because it is regarded as useless, or even troublesome, which raises challenges in modeling energy transfer. In addition, for different antennas, the radiation pattern of the back lobe varies, the established model should be general and accurate enough for most commercial off-the-shelf directional antennas.

The second challenge is how to design an effective scheduling algorithm for BACK. With respect to energy constraints, scheduling the charging path of MC is similar to solving an NP-hard traveling salesman problem (TSP). Moreover, the MC

can freely adjust its orientation in $[0, 2\pi)$, which means the number of candidate orientations for MC to choose is infinite. Note that, since the energy intensity and charging range of the back lobe are different from those of the main lobe, it is more difficult to determine not only when and where to sojourn for an MC, but its orientation.

To tackle those challenges, we first built a directional charging model considering both the main and back lobes, and we also conducted field experiments to verify the effectiveness of this charging model. Based on this, we design an effective scheduling algorithm to minimize the number of dead sensors and maximize *EUE*. The scheduling algorithm can construct an optimal charging path, enabling the MC to charge multiple sensors simultaneously utilizing both the main and back lobes at each sojourn location.

To summarize, our contributions in this paper are as follows:

- To the best of our knowledge, this is the first work to utilize both the main and back lobes to wireless charge sensors. We build a charging model with main and back lobes, which can accurately model the energy radiated by MC. In addition, this model can be reduced to a keyhole model suitable for most directional antennas.
- To solve the BACK problem, we propose a charging scheme. We show that our scheme approximates the optimal number of dead sensors with a ratio of $\max\{\frac{\beta^2}{(D_m+\beta)^2}, \frac{1}{\sqrt{2}(\sqrt{N}+1)}\}$ and the optimal *EUE* with a ratio of $\sqrt{N_l}$, where D_m and β are constants determined by the environment and the hardware parameters of chargers, N and N_l are the number of sensors and sojourn locations in the scheme, respectively.
- To evaluate our scheme, we conduct simulations and field experiments to demonstrate that on average, our scheme reduces the number of dead sensors by 49.5% and increases *EUE* by 10.2% compared to existing algorithms.

The rest of this paper is organized as follows. Section II illustrates the network model, charging models, and problem definitions. Section III presents our solutions to minimize the number of dead sensors and to maximize *EUE*. Sections IV and V evaluate our designs via simulations and field experiments. Section VI surveys the related work on WRSNs. Finally, Section VII concludes our work.

II. MODELING

In this section, we first introduce the network and charging models and formulate the BACK problem. Then the NP-hardness of the BACK problem is proved. For a quick reference, the major notations used in this paper are listed in Table I.

A. Network Model

We consider a 2D plane network (with side length L_n) with a base station (BS), N stationary rechargeable sensors $\mathcal{S} = \{s_1, s_2, \dots, s_N\}$, M candidate sojourn locations $\mathcal{L} = \{l_1, l_2, \dots, l_M\}$ [16], [17], [18], [29], and a directional MC with battery capacity B . Each sensor s_i is powered by a rechargeable battery with capacity b . Let re_i and ec_i denote the residual energy

TABLE I
IMPORTANT NOTATIONS

Notation	Description
\mathcal{S}	Set of rechargeable sensors
\mathcal{L}	Set of candidate sojourn locations
$\mathcal{S}^N(s_i)$	Set of neighbors of sensor s_i
rl_i	Current residual lifetime of sensor s_i
θ_l	Residual lifetime threshold of charging request
l_j	Sojourn location of MC
\vec{o}_{l_j}	Orientation of MC stays at sojourn location l_j
$s_j^N(s_i)$	Neighbor s_j of sensor s_i
θ_m	Beamwidth of the main lobe
θ_b	Beamwidth of the back lobe
PT	Transmission power
$PR(\cdot)$	Charging power function
G_m	Main lobe gain
G_b	Back lobe gain
D	Farthest charging distance
d	Distance between MC and sensor
N_{ds}	Number of dead sensors
EUE	Energy usage effectiveness

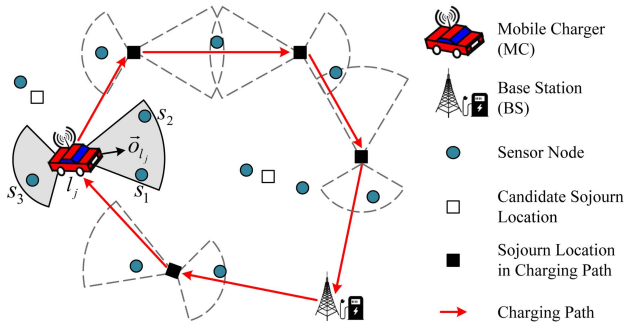


Fig. 3. Overview of the network model.

and energy consumption rate of s_i , respectively, so its residual lifetime rl_i is re_i/ec_i .

As the network operates, sensors consume their battery energy. When the residual lifetime of a sensor is lower than a given threshold θ_l , it will send a charging request $REQ_i = (t, s_i, re_i, ec_i)$ to BS, where REQ_i contains the time point t , the sensor ID s_i , its residual energy re_i , and its energy consumption rate ec_i .

Fig. 3 shows an instance of the network model. According to the received charging requests, a *charging path* is constructed by BS. In one *charging cycle*, MC departs from BS with full energy, then it moves along the charging path to visit some selected sojourn locations in some order and charges sensors wirelessly. We define the strategy of the MC as a tuple $\langle l_j, \vec{o}_{l_j} \rangle$ that denotes the sojourn location l_j and orientation \vec{o}_{l_j} of the MC. Only the sensors located in the main or back lobe can receive non-negligible energy. For example, sensors s_1, s_2 and s_3 can be charged when the MC stays at the sojourn location l_j . Before MC exhausts its energy, it returns to BS and gets recharged for the next charging cycle.

B. Charging Model

We build our directional charging model based on empirical studies and field experiments. The testbed consists of a commodity off-the-shelf wireless charger TX91501 produced

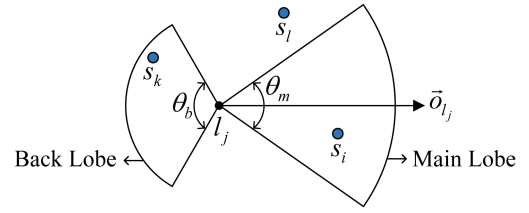


Fig. 4. Directional charging model with main and back lobes.

by Powercast [36], and a rechargeable sensor equipped with an omnidirectional antenna. We place the sensor around the charger from near to far and record the received energy. The experimental results are depicted in Fig. 2, which reveals two insights: (1) the farthest charging distance behind the charger is half of that in front of the charger (i.e., 1.3 and 2.6 m); (2) the beamwidth of the back lobe is different from that of the main lobe (i.e., $2\pi/3$ and $\pi/3$).

Therefore, we propose the directional charging model with main and back lobes as shown in Fig. 4, which generalizes the traditional directional charging model [26], [31]. For simplicity, we build a double-sector model to approximate the radiation pattern of realistic antennas. Hence, the charging range of the main and back lobes are each modeled as a sector. We apply the farthest charging distance as the radius, and the beamwidth as the angle of the sectors. Consequently, it can be seen in Fig. 4, when the orientation of charger is \vec{o}_{l_j} , s_i and s_k within charging range can be replenished, while the energy received by s_l is negligible.

In practice, since the back lobe is the energy beam of the antenna, the Friis's free space equation is also feasible in it. Therefore, by incorporating the widely accepted empirical charging model proposed in [12], [13], [26], the charging power transmitted from the charger to a sensor s_i can be given by:

$$PR(d) = \frac{G_t G_r \eta}{L_p} \left(\frac{\lambda}{4\pi(d + \beta)} \right)^2 PT, \quad (1)$$

where d is the distance between the charger and s_i , η is the rectifier efficiency, L_p is the polarization loss, λ is the average wavelength, β is a parameter to adjust the Friis's free space equation for the short distance transmission, and PT refers to the transmission power of the charger. Moreover, G_t and G_r represent the transmit gain and the receive gain, respectively.

Since sensors are equipped with an omnidirectional antenna, the receive gain G_r is an angle-independent constant. In contrast, the transmit gain G_t is a function of angle, which is defined as the ratio of the radiation intensity in a given direction to the radiation intensity produced by the omnidirectional antenna at the same power, so G_t can be expressed in a spherical coordinate system as:

$$G_t(\theta, \phi) = \eta \frac{U(\theta, \phi)}{U_o}, \quad (2)$$

where η is set to be 1 since antennas are often assumed to be lossless [42]. θ is the elevation angle from the z -axis within $[0, \pi]$, ϕ is the azimuth angle from the x -axis within $[0, 2\pi]$. $U(\theta, \phi)$

and U_o are respectively the radiation intensity of directional and omnidirectional antennas at the same power, that is, the power per unit solid angle.

For the omnidirectional antenna, it radiates power equally in all directions, so we can obtain the total transmission power of the antenna, PT , by integrating U_o over the steradian Ω :

$$PT = \iint_{\Omega} U_o d\Omega = U_o \iint_{\Omega} d\Omega = 4\pi U_o. \quad (3)$$

For the directional antenna, we place it in the center of the spherical coordinate system. Let θ_0 denote the elevation angle of the direction for power concentration, in other words, the main lobe will be targeted in the direction of the elevation angle θ_0 . Since PT is the sum of the power of all unit solid angles in the spherical coordinate system, it can also be expressed as the integral over the entire area of the $U(\theta, \phi)$:

$$PT = \iint_{\Omega} U(\theta, \phi) d\Omega = \int_0^{2\pi} \int_0^{\pi} U(\theta, \phi) \sin\theta d\theta d\phi. \quad (4)$$

By combining (2) and (4), the expression of PT with respect to the transmit gain G_t is obtained:

$$PT = \int_0^{2\pi} \int_0^{\pi} G_t(\theta, \phi) U_o \sin\theta d\theta d\phi. \quad (5)$$

Considering that the radiation intensity of the back lobe is different from that of the main lobe, we use a piecewise constant function to describe the transmit gain function $G_t(\alpha)$:

$$G_t(\alpha) = \begin{cases} G_m, & -\frac{\theta_m}{2} \leq \alpha \leq \frac{\theta_m}{2}, \\ G_b, & \pi - \frac{\theta_b}{2} \leq \alpha \leq \pi + \frac{\theta_b}{2}, \\ 0, & \text{otherwise,} \end{cases} \quad (6)$$

where α is the relative angle between the charger and the sensor. When α is within beamwidth θ_m of the main lobe, the value of $G_t(\alpha)$ is equal to the main lobe gain G_m . Similarly, when α is within beamwidth θ_b of the back lobe, its value is equal to the back lobe gain G_b . As shown in Fig. 2, the transmission power of the charger consists of two parts: the main lobe part denoted by PT_m and the back lobe part denoted by PT_b . In the same way, they can be expressed as:

$$PT_m = \int_0^{2\pi} \int_0^{\frac{\theta_m}{2}} G_m U_o \sin\theta d\theta d\phi. \quad (7)$$

$$PT_b = \int_0^{2\pi} \int_{\pi - \frac{\theta_b}{2}}^{\pi} G_b U_o \sin\theta d\theta d\phi. \quad (8)$$

Although the type of radiation is different, the transmission power is the same, so we have:

$$4\pi U_o = \int_0^{2\pi} \int_0^{\frac{\theta_m}{2}} G_m U_o \sin\theta d\theta d\phi + \int_0^{2\pi} \int_{\pi - \frac{\theta_b}{2}}^{\pi} G_b U_o \sin\theta d\theta d\phi. \quad (9)$$

The G_b can be obtained directly from the above equation:

$$G_b = \frac{2 - G_m(1 - \cos(\frac{\theta_m}{2}))}{1 + \cos(\frac{\theta_b}{2})}, \quad (10)$$

Actually, for almost all off-the-shelf chargers, manufacturers only provide the value of the main lobe gain G_m , not the back

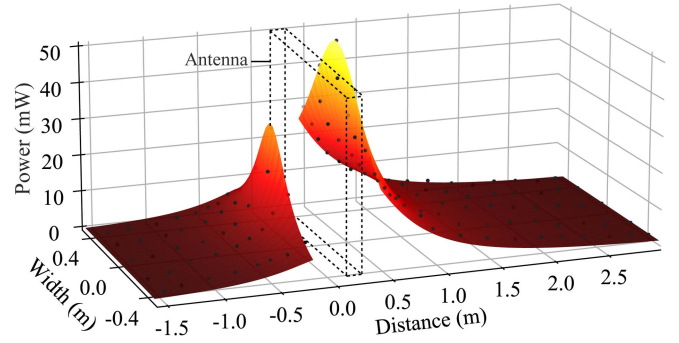


Fig. 5. Comparing experimental data (black dots) and fitted data (mesh). Fitted results are based on $\mu = 0.31$, $\beta = 0.053$, $G_m = 8$, and $G_b = 1.856$.

lobe gain G_b , because it is regarded as useless. Although the back lobe gain is not provided, it can be calculated using other known parameters.

As mentioned before, for different chargers, the radiation pattern of the back lobe varies. For directional chargers with high directivity, the charging model can be reduced to the traditional directional charging model with a back lobe beamwidth of 0 degrees. For directional chargers with many side lobes, the charging model can be reduced to the keyhole model [43], [44], which approximates all energy beams except the main lobe as a sector (i.e., $\theta_b = 2\pi - \theta_m$). Consequently, this charging model is suitable for most directional chargers.

In conclusion, the charging power transmitted from the MC to a sensor s_i is updated as:

$$PR(d, \alpha) = \begin{cases} \frac{G_m \mu}{(d+\beta)^2}, & 0 \leq d \leq D_m, -\frac{\theta_m}{2} \leq \alpha \leq \frac{\theta_m}{2}, \\ \frac{G_b \mu}{(d+\beta)^2}, & 0 \leq d \leq D_b, \pi - \frac{\theta_b}{2} \leq \alpha \leq \pi + \frac{\theta_b}{2}, \\ 0 & \text{otherwise,} \end{cases} \quad (11)$$

where d and α refer to the Euclidean distance and relative angle between MC and s_i , respectively. To simplify the expression, we set $\mu = \frac{G_r \eta}{L_p} (\frac{\lambda}{4\pi})^2 PT$ to represent some parameters. μ , G_m , and β are constants determined by the environment and the hardware parameters of chargers, G_b can be calculated by (10).

To further validate our charging model, we adopt (11) to fit the field experimental data in Fig. 2. The fitting results are shown in Fig. 5. It can be seen that the field experimental data are consistent with the fitting data of (11), which proves that the directional charging model with main and back lobes is feasible in our experimental environment.

C. Problem Formulation

In this work, we study the problem of directional charging scheduling with main and **BACK** lobes (BACK): how to carefully choose appropriate sojourn locations and orientations for directional MC with limited energy to make full use of the energy radiated by its main and back lobes, so as to jointly optimize the number of dead sensors and energy usage effectiveness (EUE).

However, there exists a tradeoff between these two objectives [13] for the following reasons: to reduce the number of dead sensors, the MC needs to simultaneously charge sensors as

much as possible to meet their charging requests. But this may lead to long-distance charging, resulting in a lower EUE . On the other hand, improving the EUE requires the MC to approach each sensor in close proximity to charge them at a very short distance. Obviously, that in turn makes it difficult to ensure that there are sufficient sensors in the MC's charging range, increasing the number of dead sensors. Therefore, the number of dead sensors and EUE cannot be optimized at the same time.

In a WSN, the deployed sensors perform various important tasks, such as sensing, collecting, and processing information. Once the energy of these sensors is exhausted, the WSN can no longer cover all monitoring areas and maintain its connectivity, potentially leading to the breakdown of the network. Therefore, our primary objective is to minimize the number of dead sensors.

Meanwhile, the battery capacity of the employed MC in a WRSN is limited. To make the energy-limited MC serve more sensors, the battery capacity of MC should be fully utilized to ensure that as much energy as possible is replenished to sensors. So our secondary objective is to maximize EUE , which is defined as follows:

$$EUE = \frac{E^{pl}}{E^{pl} + E^{tr} + E^{lo}}, \quad (12)$$

where E^{pl} is the energy eventually obtained by sensors, E^{tr} is the energy consumed to travel among sojourn locations, and E^{lo} is the energy loss during charging.

Problem 1: The primary objective is to find a directional charging scheme that utilizes both the main lobe and back lobe to minimize the number of dead sensors in one charging cycle, under the constraint of limited battery capacity and charging range of the MC, i.e.,

$$\text{minimize } N_{ds}, \quad (13)$$

subject to

$$E^{pl} + E^{tr} + E^{lo} \leq B, \quad (14)$$

$$0 \leq d \leq D_m, -\frac{\theta_m}{2} \leq \alpha \leq \frac{\theta_m}{2},$$

$$\text{or } 0 \leq d \leq D_b, \pi - \frac{\theta_b}{2} \leq \alpha \leq \pi + \frac{\theta_b}{2}. \quad (15)$$

Problem 2: The secondary objective is to find a directional charging scheme that maximizes energy usage effectiveness under the constraint of the minimum number of dead sensors, i.e.,

$$\text{maximize } EUE, \quad (16)$$

subject to

$$N_{ds} = N_{ds}^*, \quad (17)$$

where N_{ds}^* is the minimum number of dead sensors.

D. Np-Hardness of Back

We consider a special case of BACK, named BACK-S, by fixing some moving parts and angular parts in the problem formulation. We show that the decision version of BACK-S is NP-hard, and so is BACK. Consider a WRSN $G_c = (V_c, E_c)$,

where V_c contains a BS and m preselected sojourn locations. These m sojourn locations cover n to-be-charged sensors. E_c is a set of edges between each pair of sojourn locations in G_c . In BACK-S, the beamwidth of the main lobe of the MC is 2π . We assume that the residual energy of each sensor is just enough to last until the end of a charging cycle. Therefore, in one charging cycle, the sensors in BACK-S only need to be charged once, which means that MC only needs to visit each selected sojourn location once.

Theorem 1: The decision version of BACK-S is NP-hard.

Proof: We demonstrate the BACK-S problem is NP-hard by a reduction from the decision version of TSP, which is defined as follows: given a complete graph G' with $m+1$ vertices and the weight of each edge is either 1 or 2, we need to find the shortest Hamiltonian cycle C to cover all vertices such that the total weights of all edges are $m+1$. We construct an instance G_c of BACK-S, where the battery capacity of MC is $2m+1$. Each vertex (except the BS) is assigned a weight of 1, corresponding to the amount of energy that MC charges the sensors covered by this vertex. Each edge is assigned a weight of 1 or greater, which is the energy consumed by MC traveling between two sojourn locations. The decision version of BACK-S is to determine if there exists a charging path C such that the MC can charge n sensors by visiting m sojourn locations, subject to the total energy consumption in C is no more than $2m+1$. Since the battery capacity of MC is $2m+1$, the total weights of all edges in and the traveling energy consumption of MC must both be $m+1$. Thus, we can see that the optimal solution to the BACK-S problem is a solution to the TSP. The theorem thus follows. ■

III. SOLUTION

In this section, to tackle the BACK problem, we propose a scheme composed of four algorithms, among which Algorithms 1, 2, and 3 together achieve the objective of minimizing the number of dead sensors, on the basis of the minimized number of dead sensors, Algorithm 4 further maximizes the EUE .

A. Initial Path Planning Algorithm

First, we propose an initial path planning algorithm for providing a feasible charging scheduling. In order to achieve our primary objective of minimizing the number of dead sensors, we should schedule the MC to preferentially charge the sensor with the most urgent charging request. Accordingly, the basic idea of Algorithm 1 is to greedily select the energy-critical sensor with the shortest residual lifetime for charging service in each iteration. When a sensor cannot be charged before its deadline, we will try to charge it by changing the charging order. If it fails, we will adjust the MC's orientation or replace the sojourn location in the charging path to incidentally replenish energy to the dropped sensor while serving other sensors. The detailed process is demonstrated in Algorithm 1.

Algorithm 1 proceeds as follows. At first, we sort the N_r charging requests in the to-be-charged queue Q_t in increasing order of their deadlines. Shorter deadline indicates higher charging priority. That is, suppose the sorted sequence

Algorithm 1: Initial Path Planning Algorithm.

Input: A to-be-charged queue Q_t and a set of pre-determined sojourn locations \mathcal{L}

Output: An initial charging path P' and the set of dead sensors $\mathcal{N}_d(s)$

- 1 Sort all charging requests in Q_t in increasing order of their deadlines;
- 2 **for** each sensor s_i in Q_t **do**
- 3 Select the nearest sojourn location l_i to sensor s_i ;
- 4 Orientation \vec{o}_{l_i} is facing s_i (i.e., $\vec{o}_{l_i} = \vec{l}_i s_i$);
- 5 **if** $t_{l_i}^{arr} \leq TD(s_i)$ **then**
- 6 Add $\langle l_i, \vec{o}_{l_i} \rangle$ to the tail of P' ;
- 7 **continue**;
- 8 **end**
- 9 Try to insert $\langle l_i, \vec{o}_{l_i} \rangle$ into P' as the f th strategy ($1 \leq f \leq |P'|$);
- 10 **if** the insert fails **then**
- 11 Call Algorithm 2 to rescue s_i ;
- 12 **if** $t_{l_i}^{arr} > TD(s_i)$ **then**
- 13 Call Algorithm 3 to optimize P' ;
- 14 **if** $t_{l_i}^{arr} > TD(s_i)$ **then**
- 15 $\mathcal{N}_d(s) \leftarrow \mathcal{N}_d(s) \cup \{s_i\}$;
- 16 **end**
- 17 **end**
- 18 **end**
- 19 **end**
- 20 Return the initial charging path P' ;

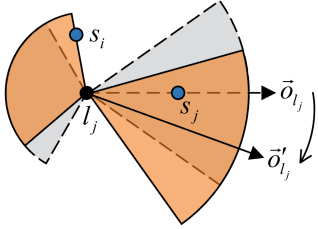


Fig. 6. Example of adjusting the MC's orientation.

is $REQ_1, REQ_2, \dots, REQ_{N_r}$, it means $TD_1 \leq TD_2 \leq \dots \leq TD_{N_r}$. Denote s_i by the sensor which sends charging request REQ_i . When trying to add s_i to the charging path, we preferentially select the nearest candidate sojourn location to s_i , and by default, the MC is facing s_i . Here, we also let l_i and \vec{o}_{l_i} denote by the corresponding sojourn location and the MC's orientation respectively when the MC serves s_i , which together constitute the strategy $\langle l_i, \vec{o}_{l_i} \rangle$. We then gradually construct an initial charging path $P' = (\langle l_1, \vec{o}_{l_1} \rangle, \langle l_2, \vec{o}_{l_2} \rangle, \dots, \langle l_{N_r}, \vec{o}_{l_{N_r}} \rangle)$ by adding $\langle l_i, \vec{o}_{l_i} \rangle$ to a partial charging path. Meanwhile, since all sensors within the charging range will be charged at the same time, we update the deadlines of all sensors covered by l_i , including s_i , after $\langle l_i, \vec{o}_{l_i} \rangle$ has been added into the charging path. Then, the charging requests in Q_t will be updated too.

For any sensor s_i , if the deadline TD_i is less than the time $t_{l_i}^{arr}$ when the MC arrives at its sojourn location l_i , it means that s_i cannot be charged in time. We call such sensor s_i as “dropped

Algorithm 2: Dropped Sensor Rescue Algorithm.

Input: A charging path P' and a strategy $\langle l_i, \vec{o}_{l_i} \rangle$ corresponding to the dropped sensor s_i

Output: An optimized path P'

- 1 Sort all neighbors in $\mathcal{S}^N(s_i)$ in increasing order of the distance from s_i ;
- 2 **for** each neighbor $s_j^N(s_i)$ in $\mathcal{S}^N(s_i)$ **do**
- 3 **if** $d_{l_j^N(s_i), s_i} \leq D_m$ **then**
- 4 Adjust the orientation $\vec{o}_{l_j^N(s_i)}$ until reaching s_i on the boundary of the charging area;
- 5 Update the strategy $\langle l_j^N(s_i), \vec{o}_{l_j^N(s_i)} \rangle$ in P' ;
- 6 **if** $t_{l_j^N(s_i)}^{arr} \leq TD(s_i)$ **then**
- 7 Add $\langle l_i, \vec{o}_{l_i} \rangle$ to the tail of P' , return P' ;
- 8 **end**
- 9 **end**
- 10 **end**
- 11 **for** each neighbor $s_j^N(s_i)$ in $\mathcal{S}^N(s_i)$ **do**
- 12 **for** each sojourn location l_j^* in L **do**
- 13 **if** l_j^* can cover s_i and s_j **then**
- 14 Add $\langle l_i, \vec{o}_{l_i} \rangle$ to the tail of P' , return P' ;
- 15 **end**
- 16 **end**
- 17 **end**
- 18 Return the optimized charging path P' ;

sensor” and it needs re-arranging a former position. Hence, we scan each former strategy to find a proper place to insert $\langle l_i, \vec{o}_{l_i} \rangle$. For a former strategy $\langle l_f, \vec{o}_{l_f} \rangle$ ($1 \leq f < i$), if inserting $\langle l_i, \vec{o}_{l_i} \rangle$ to the front of it will not cause other sensors dead, we insert $\langle l_i, \vec{o}_{l_i} \rangle$ in the front of $\langle l_f, \vec{o}_{l_f} \rangle$. Otherwise, we cannot rescue the dropped sensor s_i by only changing the charging order. In this case, Algorithms 2 and 3 will be called in turn to optimize the current P' . Once the dropped sensor s_i cannot be rescued by calling both Algorithm 2 and 3, s_i will be eventually added into the set of dead sensors $\mathcal{N}_d(s)$. Then, Algorithm 1 continues to construct the charging path until all to-be-charged sensors are tried to join the path P' .

B. Dropped Sensor Rescue Algorithm

As demonstrated in line 9 of Algorithm 1, we use Algorithm 2 to rescue the dropped sensor s_i for further minimizing the number of dead sensors. The basic idea of Algorithm 2 is to use the energy radiated from the back lobe of the MC to incidentally charge s_i while the MC serves other sensors, so as to prolong the residual lifetime of s_i . Since the MC can arbitrarily adjust its orientation at each sojourn location, we first try to change the orientation in the initial charging path so that s_i can be incidentally charged. Fig. 6 shows an example of rescuing the dropped sensor by rotating the MC. It can be seen that when the MC charges s_j with the default orientation, there is a dropped sensor s_i located outside the charging area of the MC. If we rotate the MC clockwise from \vec{o}_{l_j} to \vec{o}'_{l_j} , s_i will be replenished energy from the back lobe of the MC while the MC charges s_j .

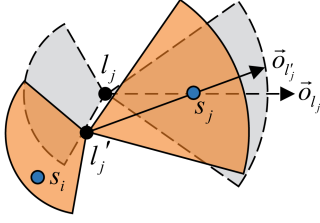


Fig. 7. Example of adjusting the MC's orientation.

If s_i cannot be rescued by adjusting the orientation, another feasible method is to select a sensor s_j in the initial path and try to replace its corresponding sojourn location with one that can simultaneously cover both s_i and s_j . As shown in Fig. 7, when the MC serves s_j , its default sojourn location is l_j , which is the nearest to s_j . Because $\angle s_j, l_j, s_i \in (\theta_m, \pi - \frac{\theta_m + \theta_b}{2})$, s_i and s_j cannot be simultaneously located within the charging range by rotating the MC. If we replace l_j with another candidate sojourn location l_j' , and determine an appropriate orientation, s_i and s_j will be charged simultaneously. Based on the above observations, we design the Dropped Sensor Rescue algorithm, and the detailed process is given in Algorithm 2.

Algorithm 2 proceeds as follows. First, we call all sensors in P' whose distance from the dropped sensor s_i is not greater than $D_m + D_b$ as neighbors of s_i . We denote by $\mathcal{S}^N(s_i)$ the set of neighbors of s_i and sort these neighbors in increasing order of the distance from s_i (i.e., $d_{s_1^N(s_i), s_i} < d_{s_2^N(s_i), s_i} < \dots$). Then, we scan each neighbor $s_j^N(s_i)$ in $\mathcal{S}^N(s_i)$ to determine whether the distance between its corresponding sojourn location $l_j^N(s_i)$ and s_i is not greater than D_m . If so, we will try to adjust its corresponding orientation to rescue s_i . The adjustment can be divided into two cases: (i) when $\angle s_j^N(s_i), l_j^N(s_i), s_i \leq \theta_m$, the MC is rotated in the direction close to s_i until reaching s_i on the boundary of the main lobe; (ii) when $\angle s_j^N(s_i), l_j^N(s_i), s_i \geq \pi - \frac{\theta_m + \theta_b}{2}$, the MC is rotated in the opposite direction from s_i until reaching s_i on the boundary of the back lobe. After adjusting the orientation, when two premise conditions: a) s_i can survive until it is added to P' ; b) it will not cause other sensors dead, are both satisfied, we will update $\langle l_j^N(s_i), \vec{o}_{l_j^N(s_i)} \rangle$ in P' and add $\langle l_i, \vec{o}_{l_i} \rangle$ to P' . When s_i cannot be rescued by adjusting the orientation, we will try to rescue it by replacing an existing sojourn location in P' with a new candidate sojourn location. We scan each neighbor $s_j^N(s_i)$ in $\mathcal{S}^N(s_i)$ to determine whether there is a nearby candidate sojourn location l_j^* that can cover both $s_j^N(s_i)$ and s_i , and judge whether two premise conditions mentioned above are both satisfied when MC is scheduled to l_j^* . If so, we will replace $\langle l_j^N(s_i), \vec{o}_{l_j^N(s_i)} \rangle$ with $\langle l_j^*, \vec{o}_{l_j^*} \rangle$, update the deadline of all sensors in P' , and add $\langle l_i, \vec{o}_{l_i} \rangle$ to the tail of P' . If there is no candidate sojourn location near all neighbor sensors in $\mathcal{S}^N(s_i)$ that can rescue s_i , Algorithm 3 will be called to optimize P' .

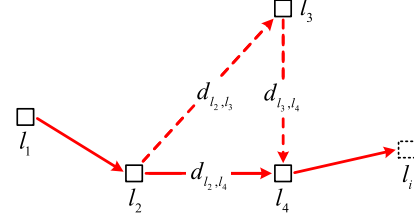


Fig. 8. Example of optimizing charging path.

Algorithm 3: Charging Path Optimization Algorithm.

Input: A charging path P' and a strategy $\langle l_i, \vec{o}_{l_i} \rangle$ corresponding to the dropped sensor s_i

Output: An optimized path P'

```

1  $P_{temp} \leftarrow P'$ ;
2 for any three adjacent sojourn locations  $l_a, l_b, l_c$  do
3    $f(l_b) = d_{l_a, l_b} + d_{l_b, l_c} - d_{l_a, l_c}$ ;
4 end
5  $l_b^* \leftarrow \arg \max f(l_b)$ ;
6 Remove strategy  $\langle l_b^*, \vec{o}_{l_b^*} \rangle$  from  $P_{temp}$ ;
7 Connect  $l_a^*$  and  $l_c^*$  in  $P_{temp}$ ;
8 for  $f \leftarrow |P_{temp}|$  to 1 do
9   Select  $\langle l_i, \vec{o}_{l_i} \rangle$  as the  $f$ th strategy to join  $P_{temp}$ ;
10  if  $N_{ds}(P_{temp}) == N_{ds}(P')$  AND
     $T_{total}(P_{temp}) < T_{total}(P')$  then
11     $P' \leftarrow P_{temp}, N_d(s) \leftarrow N_d(s) \cup \{s_i\}$ , break;
12  else
13    Remove the  $f$ th strategy from  $P_{temp}$ ;
14  end
15 end
16 Return the optimized charging path  $P'$ ;

```

C. Charging Path Optimization Algorithm

As demonstrated in line 11 of Algorithm 1, when the dropped sensor s_i cannot be rescued by calling Algorithm 2, we use Algorithm 3 to optimize the initial charging path. Our optimization objective is to preserve more time for subsequent scheduling, so that the MC can charge the sensors in the to-be-charged queue Q_t as soon as possible. Since the traveling cost of MC moving to each sojourn location is not equal, an effective way to shorten the length of the charging path is to replace the sojourn location l_{tr}^{\max} , which has the highest traveling cost in P' , with the sojourn location l_i corresponding to the dropped sensor s_i . For the replacement, the following two conditions should be satisfied: (i) the number of dead sensors brought by removing l_{tr}^{\max} will not be greater than one; (ii) after deleting l_{tr}^{\max} , s_i can be added to the charging path before its deadline, and the new path has less total traveling cost T_{total} .

We use an example to illustrate how to optimize the charging path by replacing sojourn locations. As shown in Fig. 8, $P = (\langle l_1, \vec{o}_{l_1} \rangle, \langle l_2, \vec{o}_{l_2} \rangle, \langle l_3, \vec{o}_{l_3} \rangle, \langle l_4, \vec{o}_{l_4} \rangle)$ is the initial charging path. It can be seen that l_3 is far away from its adjacent sojourn locations l_2 and l_4 , so l_3 has the highest traveling cost. Obviously, removing l_3 can not only significantly shorten the length of the charging path, but also make it probable for MC to have a great

Algorithm 4: EUE Optimization Algorithm.

Input: An initial charging path P' and the $EUE_{P'}$ obtained by the MC in P'

Output: A final charging path P and the EUE_P obtained by the MC in P

```

1  $P_{temp} \leftarrow P'$ ;
2 for  $count \leftarrow 0$  to  $\mathcal{M}$  do
3   Randomly select two sojourn locations  $l_i$  and
    $l_j (i < j)$  from  $P_{temp}$ ;
4   Take the sub-path from  $l_1$  to  $l_{i-1}$  and add it in
   order to  $P_{temp}$ ;
5   Take the sub-path from  $l_i$  to  $l_j$  and add them in
   reverse order to  $P_{temp}$ ;
6   Add the sub-path from  $l_{j+1}$  to  $l_{N_i}$  in order to
    $P_{temp}$ ;
7   if  $N_{ds}(P_{temp}) == N_{ds}(P')$  AND
    $EUE(P_{temp}) > EUE(P')$  then
8      $P' \leftarrow P_{temp}, count \leftarrow 0$ ;
9   else
10     $P_{temp} \leftarrow P', count \leftarrow count + 1$ ;
11  end
12 end
13 Return the final charging path  $P$ ;

```

chance to charge the dropped sensor s_i at sojourn location l_i before its deadline. Here, we use (18) to find the sojourn location l_{tr}^{\max} with the highest traveling cost in P' :

$$l_{tr}^{\max} = \arg \max_{l_j \in P'} (d_{l_{j-1}, l_j} + d_{l_j, l_{j+1}} - d_{l_{j-1}, l_{j+1}}). \quad (18)$$

Algorithm 3 proceeds as follows. We scan the constructed charging path P' to find l_{tr}^{\max} . Then, we remove l_{tr}^{\max} and connect its two adjacent sojourn locations. Subsequently, we scan the connected path for an appropriate position to insert the $\langle l_i, \vec{o}_i \rangle$ corresponding to s_i . If the new path satisfies the two replacement conditions mentioned above, we will add the sensor corresponding to l_{tr}^{\max} to $N_d(s)$. Otherwise, l_{tr}^{\max} will be added back to P' and s_i will be added to $N_d(s)$.

D. EUE Optimization Algorithm

After the initial charging path P' is constructed, we concentrate on the secondary objective: how to maximize the energy usage effectiveness (EUE). Recall that the total energy consumption of the MC consists of three parts: the energy obtained by sensors E^{pl} , the traveling energy consumption E^{tr} , and the energy loss during charging E^{lo} . According to (11) and (12), to achieve the maximal EUE, two following factors should be considered based on its definition: (i) shorter traveling length results in greater EUE; (ii) shorter charging distance also leads to greater EUE.

We here use a simple example to demonstrate how can we achieve the maximal EUE by jointly considering these two factors. Fig. 9(a) gives the initial charging path and its charging order is $BS \rightarrow l_1 \rightarrow l_2 \rightarrow l_3 \rightarrow l_4 \rightarrow l_5 \rightarrow BS$. It can be seen that s is located at the overlapping charging area of l_3 and l_4 . Assume

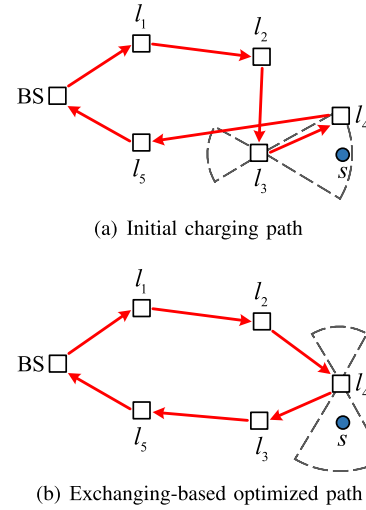


Fig. 9. Example of exchanging two sojourn locations to improve EUE.

that the residual energy of s is relatively more, it can be fully charged no matter whether MC is staying at l_3 or l_4 .

Intuitively, if we exchange the charging order of l_3 and l_4 , not only the charging path length can be reduced significantly, but s can be fully charged with a shorter charging distance when MC is staying at l_4 . The scheduling result of the optimized charging path is shown in Fig. 9(b).

From this example, it can be seen that exchanging the charging order of the initial path can jointly address the two factors mentioned above. Inspired by this observation, we design Algorithm 4, a charging order exchanging-based optimization algorithm, to maximize the EUE.

Algorithm 4 proceeds as follows. Assume there are total N_l sojourn locations in P' . We randomly select two sojourn locations l_i and $l_j (i < j)$ from P' . Then we rearrange the sub-path from l_i to l_j in reverse order while the other sub-paths remain in the same order, together forming a temporary path P_{temp} . If compared with P' , P_{temp} has the same number of dead sensors and a higher EUE, we will assign P_{temp} to P' . These process will be repeated until a continuous \mathcal{M} -times exchange of two randomly selected sojourn locations cannot lead to further improvement of EUE.

E. Relations of Algorithms

To show the execution flow of our scheduling scheme more clearly, we present a paradigm illustrating the relationship between algorithms in BACK (see Fig. 10). The definitions of the conditions (i.e. K1, K2,...) are defined in Table II.

First of all, when Algorithm 1 is called, N_r charging requests in the charging queue Q_t are sorted by their urgency. It generates an initial feasible charging path, which will be further optimized. In the meanwhile, Algorithm 2 is applied to adjust charging strategies to rescue the dropped sensor whose charging request cannot be satisfied. Nevertheless, if the dropped sensor still cannot be rescued, Algorithm 3 is executed to replace its sojourn location with the one with the highest traveling cost

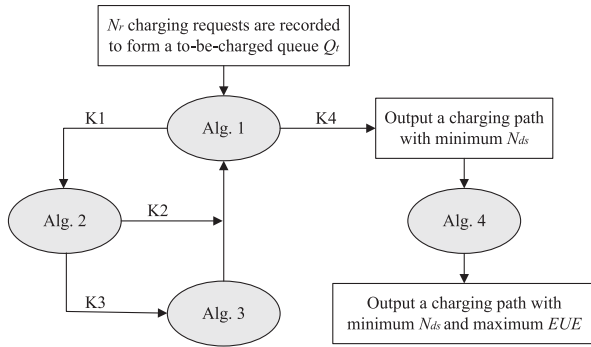


Fig. 10. Relations and converting conditions between algorithms.

TABLE II
CONDITIONS AND DEFINITIONS

Condition	Definition
K1	If a dropped sensor s_i cannot insert the charging path before it runs out of energy by adjusting the charging order, Alg. 2 will be called.
K2	After executing Alg. 2, the dropped sensor will be rescued.
K3	If the dropped sensor s_i can not be rescued by Alg. 2, Alg. 3 will be called.
K4	When all sensors are tried to add the charging path, Alg. 4 will be called.

in the charging path, thus freeing up more time for subsequent scheduling. When all sensors are tried to add the charging path and a charging path with minimum N_{ds} is obtained, Algorithm 4 is called to maximize EUE .

IV. THEORETICAL ANALYSIS

In this section, we first analyze the properties of the proposed algorithms, and then we show the time complexity of our algorithms.

A. Properties of Algorithms

Recall that the essential purpose of Algorithm 1 is to construct a charging path for the MC that minimizes the number of dead sensors. Hence, we sort the charging requests received by BS in increasing order of their urgency. In each iteration, we greedily selected the sensor with the most urgent charging request and added it to the charging path. To bound the performance, we present the approximation ratio analysis.

Theorem 2: The Algorithm 1 delivers an approximate solution to the dead sensors minimization problem with the approximation ratio of $\max\left\{\frac{\beta^2}{(D_m+\beta)^2}, \frac{1}{\sqrt{2}(\sqrt{N}+1)}\right\}$.

Proof: Consider a special case of Algorithm 1 that sensors are evenly distributed in the network. First, we analyze the relationship between the energy consumed by the MC and its battery capacity. For the optimal solution, we have:

$$E_{opt}^{pl} + E_{opt}^{tr} + E_{opt}^{lo} \leq B. \quad (19)$$

Note that, when the MC stays at a sojourn location, its transmitted power PT is spent on two parts, one part is obtained by sensors and the other part is lost during the charging process. Suppose that the charging duration of MC at each sojourn

location and traveling distance between sojourn locations are evenly distributed, the average charging duration is denoted as T_{opt}^{avg} , and the average traveling distance is denoted as d_{opt}^{avg} , we have the following equation:

$$(N - N_{ds}^*) \cdot (PT \cdot T_{opt}^{avg} + d_{opt}^{avg} \cdot c) \leq B, \quad (20)$$

where N is the number of sensors in the network, N_{ds}^* is the number of dead sensors in the optimal solution, and c is the energy consumed by traveling one unit distance.

Similarly, for our approximated solution, we have:

$$(N - N_{ds}') \cdot (PT \cdot T_{appr}^{avg} + d_{appr}^{avg} \cdot c) \leq B, \quad (21)$$

where N_{ds}' is the number of dead sensors in the approximated solution, which is the output of Algorithm 1.

Here, we consider the best case for the optimal solution: all sensors are charged close enough to the MC, and the MC visits each sojourn location with the shortest traveling distance, i.e., the uniform interval of adjacent sojourn locations. So we replace T_{opt}^{avg} and d_{opt}^{avg} by $\frac{b\beta^2}{G_m\mu}$ and $\frac{L_n}{\lceil\sqrt{N}\rceil}$. For the approximated solution, we greedily select the sensor with the shortest residual lifetime to charge it in each iteration. Consider the worst case, i.e., all sensors are located at the farthest part of the charging area of the MC and the MC visits each sojourn location with the maximum traveling distance. So we replace T_{appr}^{avg} and d_{appr}^{avg} by $\frac{b(D_m+\beta)^2}{G_m\mu}$ and $\sqrt{2}L_n$, we have:

$$(N - N_{ds}^*) \cdot \left(PT \cdot \frac{b\beta^2}{G_m\mu} + \frac{L_n}{\lceil\sqrt{N}\rceil} \cdot c \right) \leq B, \quad (22)$$

$$(N - N_{ds}') \cdot \left(PT \cdot \frac{b(D_m+\beta)^2}{G_m\mu} + \sqrt{2}L_n \cdot c \right) \leq B. \quad (23)$$

By combining (22) and (23), we have:

$$\begin{aligned} \frac{N_{ds}^*}{N_{ds}'} &\leq \frac{(N - N_{ds}^*)}{(N - N_{ds}')} \leq \frac{PT \cdot \frac{b\beta^2}{G_m\mu} + \frac{L_n}{\lceil\sqrt{N}\rceil} c}{PT \cdot \frac{b(D_m+\beta)^2}{G_m\mu} + \sqrt{2}L_n c} \\ &\leq \max \left\{ \frac{\beta^2}{(D_m+\beta)^2}, \frac{1}{\sqrt{2}(\sqrt{N}+1)} \right\}. \end{aligned} \quad (24)$$

Therefore, the number of dead sensors obtained by our solution is smaller than $\max\left\{\frac{\beta^2}{(D_m+\beta)^2}, \frac{1}{\sqrt{2}(\sqrt{N}+1)}\right\}$ of the optimal solution, and Theorem 1 is proved. ■

In Algorithm 1, when a sensor cannot be charged in time, Algorithms 2 and 3 will be called in turn to rescue it, eventually constructing an initial charging path. Our secondary objective is to maximize the EUE under the constraint that the number of dead sensors is minimized, so we designed Algorithm 4 to maximize the EUE of the initial charging path. We show the approximate ratio analysis of Algorithm 4 and the corresponding proof.

Theorem 3: The Algorithm 4 delivers an approximate solution to the EUE maximization problem with the approximation ratio of roughly $\sqrt{N_l}$.

Proof: To maximize the EUE , Algorithm 4 will try to exchange the charging order of two selected sojourn locations. We notice the basic idea of this solution is similar to the 2-opt algorithm [45], which is perhaps the most widely used

local search algorithm for the Traveling Salesman Problem. By deleting two edges of the path and reconnecting them in the other possible way, 2-opt can find the shortest path. Following a theoretical derivation similar to that shown in [46], we can prove that Algorithm 4 achieves an expected approximation ratio of roughly $\sqrt{N_l}$, where N_l is the number of sojourn locations in the charging path. Here, we omit the proof but refer readers to [46] for details. ■

B. Time Complexity of Algorithms

To analyze the complexity of our solution, the algorithms we proposed can be divided into two individual components: (i) initial charging path construction (Algorithms 1, 2, and 3); (ii) charging path optimization (Algorithm 4).

Theorem 4: The time complexity of initial charging path construction is $O(N_r^3)$.

Proof: When BS receives the charging requests, Algorithm 1 will take time $O(N_r^2)$ to sort them, where N_r is the number of charging requests. Then, in each iteration, the sensor with most urgent charging requirement is added to the initial charging path. When the sensor is dropped, Algorithm 2 will be called. The neighbors of the dropped sensor will be sorted in $\mathcal{S}^N(s_i)$, which takes time $O(N_r^2)$. Then, Algorithm 2 will take time $O(N_r)$ to rescue the dropped sensor by adjusting the orientations corresponding to $\mathcal{S}^N(s_i)$. If it fails, Algorithm 2 will take time $O(MN_r)$ to rescue the sensor again by replacing the sojourn locations, where M is the number of candidate sojourn locations. Subsequently, when the dropped sensor cannot be rescued by calling the Algorithm 2, Algorithm 3 will take time $O(N_r)$ to optimize the initial charging path. Therefore, the overall complexity of this process is $O(N_r^3)$. ■

Theorem 5: The time complexity of charging path optimization is bounded by $O(N_l^{10} \log N_l)$.

Proof: To optimize the initial charging path, Algorithm 4 iteratively exchanges the charging order of two selected sojourn locations. Many researchers have studied the time complexity of the similar local search algorithm 2-opt. In [47], Englert et al. proved the time complexity of 2-opt is bounded by $O(N_l^{10} \log N_l)$, where N_l is the number of sojourn locations in the charging path. ■

V. SIMULATIONS

In this section, we conduct simulations to verify the performance of our algorithm in terms of the number of dead sensors, *EUE* and total traveling distance.

A. Simulation Setup

We consider a WRSN consisting of 100-200 sensors, which are distributed on a 2D plane of 100 m \times 100 m, in which the BS is located at the center of the plane. In addition, 15 candidate sojourn locations are distributed on the plane. Each sensor is powered by an alkaline rechargeable battery with the capacity $b = 1.5 \text{ V} \times 2 \text{ A} \times 3,600 \text{ sec} = 10.8 \text{ KJ}$ [13]. Before the simulation starts, the sensor residual energy *re* is randomly set between $0.1b$ and $1b$. Moreover, the energy consumption

TABLE III
DEFAULT SETTINGS OF PARAMETERS

Parameters	Default values
Transmission power (<i>PT</i>)	3W
Beamwidth of the main lobe (θ_m)	$\pi/3$
Beamwidth of the back lobe (θ_b)	$2\pi/3$
Main lobe gain (G_m)	8
Back lobe gain (G_b)	1.856
Farthest charging distance of main lobe (D_m)	2.6m
Farthest charging distance of back lobe (D_b)	1.3m
μ	0.31
β	0.053

rate *ec* of each sensor randomly ranges between 0.05 J/s and 0.5 J/s. When the *ec* = 0.5 J/s (i.e., the maximal value), the residual lifetime of a sensor with full battery can reach 6 hours, thus we set the lifetime threshold $\theta_l = 6 \text{ h}$.

We assume that the battery capacity *B* of MC is 2,000 KJ, and the moving speed and the moving cost of MC are 5 m/s and 50 J/m, respectively [13]. By fitting our experiment data and referring to the hardware parameters of the equipment, the parameters of the charging model in (11) are set as: $\mu = 0.31$, $\beta = 0.053$, $G_m = 8$, $\theta_m = \pi/3$, $G_b = 1.856$, and $\theta_b = 2\pi/3$. According to the field experiment we performed in Fig. 2, we set the farthest charging distance of the main and back lobes as 2.6 m and 1.3 m, respectively. The energy transmission power of the MC is set to 3 W. Table III lists the parameters used in the experiments. Unless otherwise specified, these parameters will be adopted in the default setting.

B. Baseline Setup

To evaluate the performance of our proposed BACK algorithm, we compare it with the following charging algorithms.

Main Lobe Charging (MLC) [29] algorithm is a directional charging algorithm that only utilizes the main lobe. MLC considers the anisotropy of the received energy, and its objective is to jointly optimize the number of dead sensors and *EUE*.

Lifetime Maximization Charging (LMC) algorithm is also a directional charging algorithm that only utilizes the main lobe. However, the objective of LMC is to minimize the number of dead sensors. Therefore, LMC does not include the optimization algorithm based on the idea of exchanging sojourn locations.

Nearest-Job-Next with Preemption (NJNP) [23] is an on-demand charging algorithm for the single-sensor charging model. To save time and energy spent traveling, NJNP always serves the nearest sensor with a charging request.

C. Performance Comparisons

In this section, we evaluate the performance of our proposed scheme by comparing it with the three comparison algorithms under different number of sensors *N* and the beamwidth of the back lobe θ_b .

1) *Impact of the number of sensors N:* Fig. 11(a) shows the influence of the *N* on the number of dead sensors. As the number of sensors in the network increases, the N_{ds} yielded by all algorithms increases. However, we can see that BACK outperforms other algorithms by an average of 51.9%. Moreover, when the number of sensors is larger, the advantage of the BACK

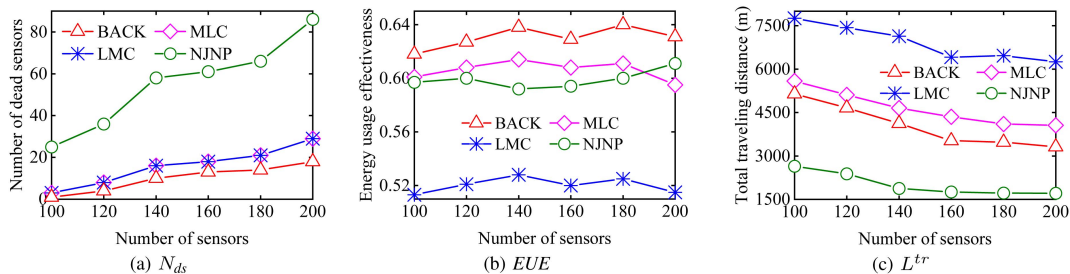


Fig. 11. Performance comparisons by varying the number of sensors.

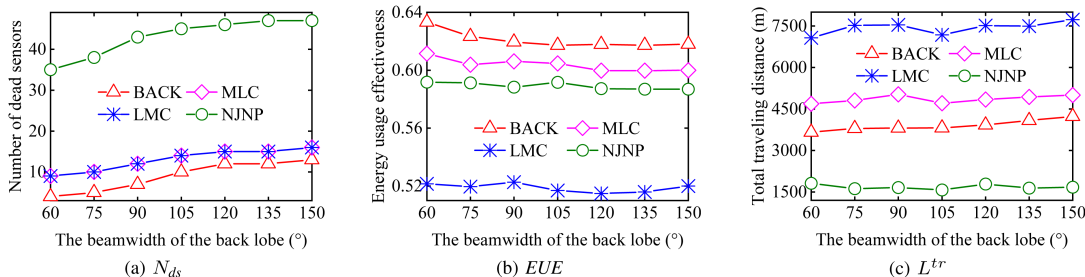


Fig. 12. Performance comparisons by varying θ_b .

algorithm is even more obvious. This is because with a constant network size, a higher number of sensors results in a denser distribution of sensors near the sojourn location. Consequently, the distances between sensors are more likely to be less than 2.6 m , allowing the BACK algorithm to simultaneously charge multiple sensors utilizing both the main and back lobes, and the advantages of the back lobe will be more obvious.

Fig. 11(b) compares another performance metric, EUE . BACK achieves 10.2% higher EUE than other algorithms on average. The rationale behind this is two-fold: (i) BACK makes full use of the energy radiated from the back lobe to charge more sensors simultaneously by adjusting the MC's orientation; (ii) the charging order exchanging-based EUE optimization algorithm can further shorten the traveling distance and reduce energy loss. Moreover, by comparing MLC and LMC, we find that although none of them take into account the energy radiated by the back lobe, LMC has a lower EUE due to the absence of EUE optimization.

Then, we measure the total traveling distance. From Fig. 11(c), we can see that NJNP has the best performance. The reason is that NJNP causes much larger N_{ds} than other algorithms do, the total traveling distance generated by NJNP is the shortest. Fig. 11(c) also shows that BACK has a shorter traveling distance than MLC and LMC. This is because full use of the back lobe can reduce the number of sojourn locations visited, thus effectively shortening the traveling distance.

2) *Impact of the beamwidth of the back lobe θ_b* : We fix the number of sensors at 150 and further investigate the impact of θ_b . Fig. 12(a) shows the comparison of N_{ds} . On average, BACK outperforms other algorithms by 47%. It also can be seen that with the increase of θ_b , the N_{ds} generated by all algorithms increases. This is because, with the increase of θ_b , the back lobe energy gradually disperses, making the energy intensity

received by the sensors covered by the back lobe also decrease. Therefore, it is difficult for these sensors to obtain sufficient energy to guarantee their survival.

Fig. 12 compares the other two metrics, EUE and traveling distance. In Fig. 12(b), the EUE yielded by all algorithms decreases slightly as θ_b increases. The reason is that the more dispersed the back lobe energy is, the smaller the ratio of the energy received by sensors to the total energy radiated by the back lobe is, resulting in more energy loss in the charging process. Fig. 12(c) shows that the change of θ_b does not significantly influence the traveling distance of all algorithms.

Combining the results of Fig. 12, we can observe that the smaller the beamwidth of the back lobe, the more energy the sensor located in the back lobe region can receive from the more concentrated energy beam. Therefore, chargers equipped with antennas with larger back lobe gain can provide better charging service.

VI. FIELD EXPERIMENTS

To better verify the performance of our proposed BACK scheme, we conduct field experiments in this section.

A. Testbed

Our testbed, depicted in Fig. 13, comprises a robot car equipped with a TX91501 Powercast wireless charger, eight rechargeable sensors equipped with omnidirectional antennas, and an access point (AP) that connects to a laptop for reporting the collected data from the sensors. The robot car operates at a constant speed of 0.3 m/s and consumes energy at a rate of 5.59 J/m [24]. Additionally, it is equipped with a GPS and a camera for recording and positioning purposes. The sensors are

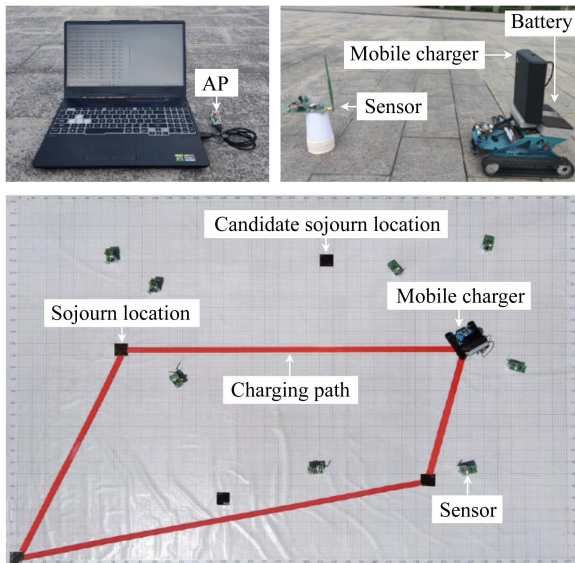


Fig. 13. Testbed.

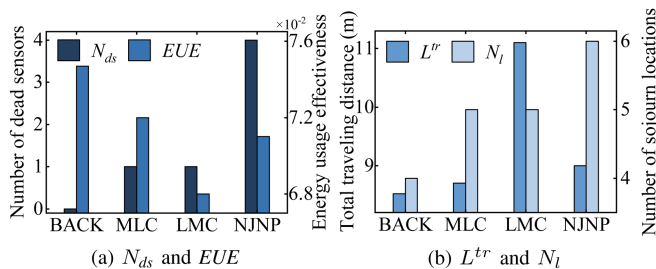


Fig. 14. Performance comparisons.

deployed within a $400 \text{ cm} \times 300 \text{ cm}$ area, with their respective coordinates as follows: (70, 250), (100, 225), (115, 150), (240, 75), (275, 240), (325, 75), (340, 260), and (360, 160). Significantly, Figure 13 provides a visual representation of the charging path constructed by BACK, which enhances the intuitive understanding of the charging process.

B. Experimental Results

Fig. 14 illustrates a comparison of four metrics: N_{ds} , EUE , L^{tr} , and N_l , where N_l represents the number of sojourn locations in the charging path. Consistent with the simulation results, the BACK algorithm yields the least number of dead sensors and achieves the highest EUE . In addition, the BACK has the shortest traveling distances and the least number of sojourn locations. The reason can be explained by Fig. 15, which depicts the charging paths constructed by the four algorithms. By making full use of the main and back lobes, we can observe that BACK covers a larger number of sensors at each sojourn location. As a result, it significantly reduces the overall number of sojourn locations visited, leading to shorter traveling distances and ensuring the survival of all sensors.

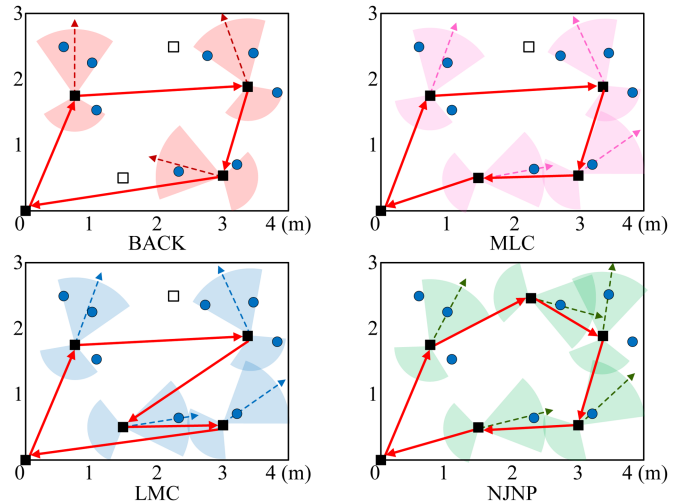


Fig. 15. Charging paths constructed by four algorithms.

VII. RELATED WORK

In general, the prior charging methods in WRSNs are two categories based on the type of antenna the charger is equipped with: omnidirectional charging [5], [13], [14], [15], [16], [17], [18], [19], [20] and directional charging [26], [27], [28], [29], [30], [31], [33], [34].

A. Omnidirectional Charging

Most previous studies employ mobile chargers equipped with omnidirectional antennas to charge sensors. Zhou et al. [5] proposed a self-sustained WSN by integrating multi-source energy harvesting with omnidirectional charging scheduling, effectively addressing the challenge of energy provisioning under complex weather conditions. In [13], Liu et al. designed a partial charging mechanism and proposed an omnidirectional charging scheduling to jointly optimize the number of dead sensors and energy usage effectiveness. In addition, to further improve the charging performance, the sensor lifetime maximization problem is also explored [14]. Xu et al. [15] studied the effective scheduling of multiple omnidirectional chargers to charge sensors, so as to minimize the maximum charging delay. For mobile devices with non-deterministic mobility, Liu et al. [16] introduced hotspots, which are frequently visited by mobile devices, and scheduled an omnidirectional charger to charge devices at hotspots, aiming to maximize the total reward in one charging cycle. Yang et al. [17] studied how to schedule an omnidirectional charger in a risk-averse view, so as to improve the network robustness. In [18], Sun et al. paid close attention to trading off charging and sensing tasks and studied the optimization problem of omnidirectional charging scheduling. Jia et al. [19] designed the charging path of an omnidirectional charger to minimize the energy cost for both charging and movement, such that the different charging demand of each sensor is satisfied. In addition, Ma et al. [20] considered the wave interference in the concurrent charging scenario and they proposed a concurrent charging scheme to take full advantage of

the high power caused by constructive interference to enhance the charging efficiency.

Nevertheless, omnidirectional antennas broadcast energy in all directions, resulting in low energy intensity within the charging range.

B. Directional Charging

There exist some studies employing chargers equipped with directional antennas. Dai et al. [26] proposed the first scheme for wireless charger placement with optimized charging utility. Then, Wang et al. [27] studied how to deploy heterogeneous directional chargers in a network with obstacles, so as to maximize the overall charging utility. In addition, directional chargers with limited mobility have been explored to further improve charging performance [28]. In [29], Lin et al. considered how to minimize charging delay by utilizing the anisotropic energy receiving property of sensors in directional charging. Sun et al. [30] concentrated on utilizing hybrid chargers and using freeloading directional chargers to recycle the wasted energy, so as to improve the energy efficiency of the whole network. Dai et al. [31] studied how to schedule a directional charger to recharge sensors in an arbitrary simple polygon with the charger only allowed to move along the polygon boundaries. Then, they also studied how to deploy multiple directional chargers to achieve omnidirectional charging [32]. Wu et al. [33] focused on cooperative scheduling in directional wireless charging, taking into account the spatial occupancy of the sensors. Their objective was to minimize the total cost of the charging system. In [34], Yu et al. considered the connectivity issues for directional chargers, and proposed a deployment scheme to maximize charging utility.

However, they overlooked that the back lobe has significant energy, which is wasted. In this paper, we make the first attempt to utilize both the main and back lobes for mobile charging, which shows the significant impact of utilizing the back lobe on enhancing charging performance.

VIII. CONCLUSION

The key novelty of this paper is to propose the first charging scheduling scheme which considers the back lobe in directional charging. The main contribution of this paper is to establish the directional charging model with the main and back lobes and verify the model by conducting experiments. Based on this model, we concentrate on jointly optimizing the number of dead sensors and energy usage effectiveness. To this end, we propose a scheme consisting of four sub-algorithms. Theoretical analysis shows that our scheme can approximate the minimum number of dead sensors and the maximum energy efficiency with a close ratio. Moreover, our simulation and field experimental results show that our proposed scheme significantly outperforms the existing algorithms.

REFERENCES

- [1] A. Cohen, X. Shen, J. Torrellas, J. Tuck, and Y. Zhou, "Inter-disciplinary research challenges in computer systems for the 2020s," Nat. Sci. Found., Alexandria, VA, USA, Tech Rep., 2018. [Online]. Available: <https://dl.acm.org/doi/book/10.5555/3297279>
- [2] Y. Hu et al., "Experience: Practical indoor localization for malls," in *Proc. 28th Annu. Int. Conf. Mobile Comput. Netw.*, 2022, pp. 82–93.
- [3] A. Kurs, A. Karalis, R. Moffatt, J. D. Joannopoulos, P. Fisher, and M. Soljačić, "Wireless power transfer via strongly coupled magnetic resonances," *Science*, vol. 317, no. 5834, pp. 83–86, 2007.
- [4] Y. Yang and C. Wang, *Wireless Rechargeable Sensor Networks*. Berlin, Germany: Springer, 2015.
- [5] P. Zhou, C. Wang, and Y. Yang, "Design of self-sustainable wireless sensor networks with energy harvesting and wireless charging," *ACM Trans. Sensor Netw.*, vol. 17, no. 4, pp. 1–38, 2021.
- [6] S. Wu, H. Dai, L. Xu, L. Liu, F. Xiao, and J. Xu, "Comprehensive cost optimization for charger deployment in multi-hop wireless charging," *IEEE Trans. Mobile Comput.*, vol. 22, no. 8, pp. 4563–4577, Aug. 2023.
- [7] W. Ouyang, M. S. Obaidat, X. Liu, X. Long, W. Xu, and T. Liu, "Importance-different charging scheduling based on matroid theory for wireless rechargeable sensor networks," *IEEE Trans. Wireless Commun.*, vol. 20, no. 5, pp. 3284–3294, May 2021.
- [8] X. Liu, P. Lin, T. Liu, T. Wang, A. Liu, and W. Xu, "Objective-variable tour planning for mobile data collection in partitioned sensor networks," *IEEE Trans. Mobile Comput.*, vol. 21, no. 1, pp. 239–251, Jan. 2022.
- [9] M. Zhao, J. Li, and Y. Yang, "A framework of joint mobile energy replenishment and data gathering in wireless rechargeable sensor networks," *IEEE Trans. Mobile Comput.*, vol. 13, no. 12, pp. 2689–2705, Dec. 2014.
- [10] X. Fan et al., "Towards flexible wireless charging for medical implants using distributed antenna system," in *Proc. 26th Annu. Int. Conf. Mobile Comput. Netw.*, 2020, pp. 1–15.
- [11] S. He, K. Hu, S. Li, L. Fu, C. Gu, and J. Chen, "A robust RF-based wireless charging system for dockless bike-sharing," *IEEE Trans. Mobile Comput.*, early access, Mar. 13, 2023, doi: [10.1109/TMC.2023.3255980](https://doi.org/10.1109/TMC.2023.3255980).
- [12] S. He, J. Chen, F. Jiang, D. K. Y. Yau, G. Xing, and Y. Sun, "Energy provisioning in wireless rechargeable sensor networks," *IEEE Trans. Mobile Comput.*, vol. 12, no. 10, pp. 1931–1942, Oct. 2013.
- [13] T. Liu, B. Wu, S. Zhang, J. Peng, and W. Xu, "An effective multi-node charging scheme for wireless rechargeable sensor networks," in *Proc. 39th IEEE Int. Conf. Comput. Commun.*, 2020, pp. 2026–2035.
- [14] J. Liu et al., "Maximizing sensor lifetime via multi-node partial-charging on sensors," *IEEE Trans. Mobile Comput.*, vol. 22, no. 11, pp. 6571–6584, Nov. 2023.
- [15] W. Xu, W. Liang, X. Jia, H. Kan, Y. Xu, and X. Zhang, "Minimizing the maximum charging delay of multiple mobile chargers under the multi-node energy charging scheme," *IEEE Trans. Mobile Comput.*, vol. 20, no. 5, pp. 1846–1861, May 2021.
- [16] T. Liu, B. Wu, W. Xu, X. Cao, J. Peng, and H. Wu, "RLC: A reinforcement learning-based charging algorithm for mobile devices," *ACM Trans. Sensor Netw.*, vol. 17, no. 4, pp. 1–23, 2021.
- [17] W. Yang et al., "Robust wireless rechargeable sensor networks," *IEEE/ACM Trans. Netw.*, vol. 31, no. 3, pp. 949–964, Jun. 2023.
- [18] Y. Sun et al., "Trading off charging and sensing for stochastic events monitoring in WRSNs," *IEEE/ACM Trans. Netw.*, vol. 30, no. 2, pp. 557–571, Apr. 2022.
- [19] R. Jia, J. Wu, J. Lu, M. Li, F. Lin, and Z. Zheng, "Energy saving in heterogeneous wireless rechargeable sensor networks," in *Proc. 41th IEEE Int. Conf. Comput. Commun.*, 2022, pp. 1838–1847.
- [20] Y. Ma, D. Wu, M. Ren, J. Peng, J. Yang, and T. Liu, "Concurrent charging with wave interference," in *Proc. IEEE 42nd Int. Conf. Comput. Commun.*, 2023, pp. 1–10.
- [21] W. You et al., "A practical charger placement scheme for wireless rechargeable sensor networks with obstacles," *ACM Trans. Sensor Netw.*, vol. 20, 2023, Art. no. 11.
- [22] Y. Sun et al., "Charging dynamic sensors through online learning," in *Proc. 42nd IEEE Int. Conf. Comput. Commun.*, 2023, pp. 1–10.
- [23] L. He, L. Kong, Y. Gu, J. Pan, and T. Zhu, "Evaluating the on-demand mobile charging in wireless sensor networks," *IEEE Trans. Mobile Comput.*, vol. 14, no. 9, pp. 1861–1875, Sep. 2015.
- [24] C. Wang, J. Li, F. Ye, and Y. Yang, "Recharging schedules for wireless sensor networks with vehicle movement costs and capacity constraints," in *Proc. IEEE 11th Annu. Int. Conf. Sens. Commun. Netw.*, 2014, pp. 468–476.
- [25] Z. Wang, L. Duan, and R. Zhang, "Adaptively directional wireless power transfer for large-scale sensor networks," *IEEE J. Sel. Areas Commun.*, vol. 34, no. 5, pp. 1785–1800, May 2016.
- [26] H. Dai, X. Wang, A. X. Liu, H. Ma, G. Chen, and W. Dou, "Wireless charger placement for directional charging," *IEEE/ACM Trans. Netw.*, vol. 26, no. 4, pp. 1865–1878, Aug. 2018.
- [27] X. Wang et al., "Practical heterogeneous wireless charger placement with obstacles," *IEEE Trans. Mobile Comput.*, vol. 19, no. 8, pp. 1910–1927, Aug. 2020.

- [28] H. Dai et al., "Placing wireless chargers with multiple antennas," in *Proc. IEEE 19th Annu. Int. Conf. Sens. Commun. Netw.*, 2022, pp. 479–487.
- [29] C. Lin, Z. Yang, H. Dai, L. Cui, L. Wang, and G. Wu, "Minimizing charging delay for directional charging," *IEEE/ACM Trans. Netw.*, vol. 29, no. 6, pp. 2478–2493, Dec. 2021.
- [30] Y. Sun et al., "Recycling wasted energy for mobile charging," in *Proc. IEEE 29th Int. Conf. Netw. Protoc.*, 2021, pp. 1–11.
- [31] H. Dai et al., "Area charging for wireless rechargeable sensors," in *Proc. IEEE 29th Int. Conf. Comput. Commun. Netw.*, 2020, pp. 1–9.
- [32] H. Dai, Y. Zhang, X. Wang, A. X. Liu, and G. Chen, "Omnidirectional chargability with directional antennas," *IEEE Trans. Mobile Comput.*, early access, Jul. 11, 2023, doi: [10.1109/ICNP.2016.7784435](https://doi.org/10.1109/ICNP.2016.7784435).
- [33] S. Wu, H. Dai, L. Liu, L. Xu, F. Xiao, and J. Xu, "Cooperative scheduling for directional wireless charging with spatial occupation," *IEEE Trans. Mobile Comput.*, early access, Oct. 17, 2022, doi: [10.1109/TMC.2022.3214979](https://doi.org/10.1109/TMC.2022.3214979).
- [34] N. Yu, H. Dai, G. Chen, A. X. Liu, B. Tian, and T. He, "Connectivity-constrained placement of wireless chargers," *IEEE Trans. Mobile Comput.*, vol. 20, no. 3, pp. 909–927, Mar. 2021.
- [35] C. A. Balanis, *Antenna Theory: Analysis and Design*. Hoboken, NJ, USA: Wiley, 2015.
- [36] "Powercast." Accessed: 2023. [Online]. Available: <http://www.powercastco.com>
- [37] "Alien technology." Accessed: 2023. [Online]. Available: <http://www.alientechnology.com>
- [38] "Taoglas." Accessed: 2023. [Online]. Available: <http://taoglas.com>
- [39] N. Javanbakht, R. E. Amaya, J. Shaker, and B. Syrett, "Side-lobe level reduction of half-mode substrate integrated waveguide leaky-wave antenna," *IEEE Trans. Antennas Propag.*, vol. 69, no. 6, pp. 3572–3577, Jun. 2021.
- [40] N. Javanbakht, M. S. Majedi, and A. R. Attari, "Thinned array inspired quasi-uniform leaky-wave antenna with low side-lobe level," *IEEE Antennas Wireless Propag. Lett.*, vol. 16, pp. 2992–2995, 2017.
- [41] F. C. Chen, H. T. Hu, R. S. Li, Q. X. Chu, and M. J. Lancaster, "Design of filtering microstrip antenna array with reduced sidelobe level," *IEEE Trans. Antennas Propag.*, vol. 65, no. 2, pp. 903–908, Feb. 2017.
- [42] M. Z. Hasan and H. Al-Rizzo, "Beamforming optimization in Internet of Things applications using robust swarm algorithm in conjunction with connectable and collaborative sensors," *Sensors*, vol. 20, no. 7, 2020, Art. no. 2048.
- [43] T. Bai and R. W. Heath, "Coverage and rate analysis for millimeter-wave cellular networks," *IEEE Trans. Wireless Commun.*, vol. 14, no. 2, pp. 1100–1114, Feb. 2015.
- [44] A. Thornburg, T. Bai, and R. W. Heath, "Performance analysis of outdoor mmWave ad hoc networks," *IEEE Trans. Signal Process.*, vol. 64, no. 15, pp. 4065–4079, Aug. 2016.
- [45] D. S. Johnson and L. A. McGeoch, "The traveling salesman problem: A case study in local optimization," *Local Search Combinatorial Optim.*, vol. 1, no. 1, pp. 215–310, 1997.
- [46] C. Engels and B. Manthey, "Average-case approximation ratio of the 2-opt algorithm for the TSP," *Operations Res. Lett.*, vol. 37, no. 2, pp. 83–84, 2009.
- [47] M. Englert, H. Röglin, and B. Vöcking, "Worst case and probabilistic analysis of the 2-opt algorithm for the TSP," *Algorithmica*, vol. 68, no. 1, pp. 190–264, 2014.



Meixuan Ren (Student Member, IEEE) received the BS degree from the Department of Mathematics, Sichuan Normal University, China, in 2020, and the ME degree from the Department of Computer Science and Technology, Sichuan Normal University, China, in 2023. She is currently working toward the PhD degree with the Department of Computer Science and Technology, Nanjing University, China. Her research interests include wireless charging and the Internet of Things.



Dié Wu received the BS degree in information security and the PhD degree in computer architecture from the Electronic Science and Technology of China, in 2011 and 2018, respectively. From 2016 to 2017, he was a visiting PhD student with Nanyang Technological University, Singapore. He is currently an assistant professor with the College of Computer Science, Sichuan Normal University, Chengdu, China. His research interests include RFID systems, wireless networks, and pervasive computing.



Jing Xue received the BS degree in electronic and information engineering from the Beijing University of Posts and Telecommunications, China, in 2019. She is currently working toward the master's degree in electronic and information engineering with Sichuan Normal University. Her research interests include wireless charging and wireless sensor networks.



Jingwen Li received the bachelor's degree in computer science from the University of Electronic Science and Technology of China, China, in 2018, and the PhD degree from the Department of Industrial Systems Engineering and Management, National University of Singapore, in 2022. She is currently a lecturer with the Department of Computer Science, Sichuan Normal University. Her research focuses on deep reinforcement learning for combinatorial optimization problems, especially for vehicle routing problems.



Sun Mao received the PhD degree in communication and information systems from the University of Electronic Science and Technology of China, Chengdu, China, in 2020. From 2018 to 2019, he was a visiting PhD student with the University of Oslo, Oslo, Norway. He is currently a lecturer with the College of Computer Science, Sichuan Normal University. His research interests include simultaneous wireless information and power transfer, mobile edge computing, and intelligent reflecting surface-assisted wireless networks.



Wenzheng Xu (Member, IEEE) received the BSc, ME, and PhD degrees in computer science from Sun Yat-Sen University, Guangzhou, China, in 2008, 2010, and 2015, respectively. He is currently an associate professor with Sichuan University. He was a visitor with the Australian National University and Chinese University of Hong Kong. His research interests include Internet of Things, UAV networking, mobile computing, approximation algorithms, combinatorial optimization, online social networks, and graph theory.



Tang Liu (Member, IEEE) received the BS degree in computer science from the University of Electronic and Science of China, China, in 2003, and the MS and PhD degrees in computer science from Sichuan University in 2009 and 2015, respectively. Since 2003, he has been with the College of Computer Science, Sichuan Normal University, where he is currently a professor. He has authored more than 40 scientific papers in several journals and conferences, including *IEEE INFOCOM*, *IEEE Transactions on Mobile Computing*, *IEEE/ACM Transactions on Networking*, *IEEE Transactions on Wireless Communications*, *ACM Transactions on Sensor Networks*, and *IEEE IPDPS*. His research interests include wireless charging, Internet of Things, and wireless sensor networks. He is a senior member of China Computer Federation.